ACS OMEGA

Open Access

http://pubs.acs.org/journal/acsodf

Article

Integrative Analyses of Single-Cell RNA-Sequencing and Bulk RNA-Sequencing Reveal Prognostic Markers of Peripheral Blood Mononuclear Cells in Patients with Cardiogenic Shock Receiving Venous-Arterial Extracorporeal Membrane Oxygenation Support Collected before Venous-Arterial Extracorporeal Membrane Oxygenation Establishment

Lei Wang, Guodong Zhong,*,⊥ and Liangwan Chen*,⊥

Cite This: *ACS Omega* 2025, 10, 637−654

Read Online

ACCESS | Metrics & More | Article Recommendations | Supporting Information

ABSTRACT: The impact of changes in peripheral blood mononuclear cells (PBMCs) on the prognosis of patients with cardiogenic shock (CS) receiving venous-arterial extracorporeal membrane oxygenation (VA-ECMO) remains unclear. A single-cell RNA-sequencing (scRNA-seq) and a bulk RNA-sequencing (bulk RNA-seq) data sets of pre-ECMO PBMCs of CS patients were obtained from the gene expression omnibus database, which were analyzed using the "Seurat" and "limma" packages, respectively. The counts of different PMBC cell types, differential expression genes (DEGs), pathway enrichment analysis, cell−cell communication analysis, pseudotime analysis, and immune cell infiltration analysis were compared between VA-ECMO groups with different prognoses. The intersectional DEGs of the two data sets were screened. PBMCs were collected from VA-ECMO patients for experimental verification. For scRNA-seq analysis, ten kinds of PBMCs were identified, and B and NK/NKT cells which had significant differences in cell counts across groups were further divided into four subsets. The counts of B and NK/NKT cells with high expression levels of HSPA1B were higher in the poor-prognosis group, which was consistent with the bulk RNA-seq analysis. Pseudotime analysis also indicated that B-HSPA1B cells gradually increased in the poor-prognosis group. HSPA1B was found to be the intersectional upregulated DEG in both data sets, which was consistent with the experimental verification using clinical samples. The increased counts of B and NK/NKT cells as well as high expression levels of HSPA1B in these cell types or in the total pre-ECMO PBMCs were predictors of poor prognosis.

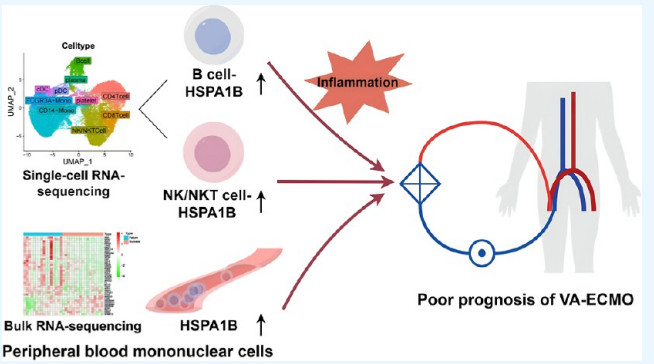

1. INTRODUCTION

Venous-arterial extracorporeal membrane oxygenation (VA-ECMO) is a crucial method of cardiopulmonary support for patients experiencing refractory cardiogenic shock (CS). However, VA-ECMO is associated with numerous complications, such as bleedings, infections, and lower limb ischemia,[1] and the survival rate of patients discharged from the hospital is notably low, ranging only between 35% and 45%.[2] The findings of a recent large randomized controlled study indicated that for patients with severe CS, there was no significant difference in complications and all-cause mortality between immediate VA-ECMO support and conservative treatment (downstream use of VA-ECMO was allowed).[3] Furthermore, resources for ECMO are limited, and the cost of ECMO is high. Therefore, it is imperative to predict whether VA-ECMO will be beneficial for patients with CS prior to establishing VA-ECMO.

The impact of changes in the counts and functions of immune cells in peripheral blood on the prognosis of patients with CS receiving VA-ECMO support before VA-ECMO establishment remains unclear. Exploring immune cells and biomarkers related to VA-ECMO prognosis may potentially predict patient outcomes and provide relevant immunotherapy. Therefore, we aimed to analyze the influence and predictive efficacy of immune cell counts and functions on patient prognosis prior to VA-ECMO establishment as well as explore possible interventions to enhance the successful application of VA-ECMO through

Received: August 13, 2024
Revised: December 5, 2024
Accepted: December 20, 2024
Published: December 31, 2024

https://doi.org/10.1021/acsomega.4c07339
ACS Omega 2025, 10, 637−654

gene expression omnibus (GEO) data sets. Additionally, blood samples were collected from VA-ECMO patients for peripheral blood mononuclear cell (PBMC) isolation, and mRNA and protein levels of key PBMC markers were compared and verified between groups with different prognoses.

2. METHODS

2.1. Data Download and Processing. Data sets pertaining to VA-ECMO prognoses were retrieved from the GEO database. Specifically, a single-cell RNA-sequencing (scRNA-seq) data set GSE127221 and a bulk RNA sequencing (bulk RNA-seq) data set GSE93101 were obtained. The expression matrices and clinical information on these two data sets were downloaded and analyzed.

2.2. Analysis of scRNA-Seq Data. *2.2.1. Processing of scRNA-Seq Data.* The "Seurat" package was utilized to process and analyze the scRNA-seq data through the following steps: (1) object construction: conversion of the scRNA-seq data into Seurat objects. (2) Data filtering, specifically quality control (QC): setting thresholds to filter genes and cells in order to exclude low-quality cells, including genes expressed in less than 10 cells; cells with nFeature_RNA less than 200 and more than 2500; cells with a proportion of mitochondrial genes greater than 25%; cells with a proportion of erythrocyte genes greater than 10%. (3) Data standardization: utilizing the "FindVariableFeatures" function to identify the top 2000 highly variable genes (HVGs) after QC. (4) Data dimensionality reduction and clustering: selecting the first 2000 HVGs as inputs for principal component analysis (PCA), utilizing the "ElbowPlot" function to determine the number of important principal components (PCs) for subsequent cluster analysis. Additionally, batch effects were observed through the PCA plot. The "FindClusters" algorithm was employed to identify cell types with a resolution of 1 and the "DimPlot" function was used to visualize cell types.

2.2.2. Annotations of Cell Clusterings. The "SingleR" package and the "Sc-Type" method were utilized to automatically annotate cell clusterings.[4] Additionally, manual annotation was performed for each cell clustering using the "FindAllMarkers" function to identify differentially expressed genes (DEGs) with a screening threshold of $|\log 2\ FC| > 0.4$, $P < 0.05$, and an expression ratio of DEGs ≥ 0.25 in the cell clusterings. The specific cell types expressing each DEG were retrieved through Cellmarker online Web site (http://biocc.hrbmu.edu.cn/CellMarker/index.jsp) to determine cell types of each cell clustering subsequently. The results of annotations for cell clusterings were visualized using the "DimPlot" function, while the expression distributions of marker genes for cell clusterings or cell types were visualized using "FeaturePlot", "DotPlot", "DoHeatmap", and "VlnPlot" functions.

2.2.3. Comparison of the Cellular Proportions, DEGs, and Pathway Enrichment among Various Cell Types in Groups with Different VA-ECMO Prognoses. The cellular proportions of different cell types in groups with varying VA-ECMO prognoses were compared by using bar graphs. The "FindMarkers" function was utilized to compare the DEGs of different cell types between the various prognostic groups, and these comparisons were visually represented with volcano plots. Subsequently, the "ClusterProfiler" package and the hallmark pathway gene set were employed for gene set variation analysis (GSVA) to investigate the pathway enrichment of DEGs.

2.2.4. Cell−Cell Communication Analysis. The "CellChat" package was utilized to elucidate the interactions between different cell types. Standardized data from Seurat were imported into CellChat, and intercellular communication was inferred based on CellChat's built-in ligand−receptor database. The functions "computeCommunProb" and "computeCommunProbPathway" were employed to identify potential interactions and pathways between cells. Additionally, the "filterCommunication" function was applied to exclude cell communications of cell types with less than 10 cells in order to enhance the stability of the analysis.

2.2.5. Further Subcategories of Cell Types Exhibiting Significant Differences in Cell Counts among Various Prognostic Groups. Further subcategories were conducted to analyze cell types with significant differences in cell counts across different prognostic groups. Data standardization, dimensionality reduction and clustering, and identification of marker genes for specific cell types were performed based on the scRNA-seq data. Manual annotation was utilized to annotate the cell clusterings. The cell proportions of different cell types in different prognostic groups were compared and presented by using bar graphs.

Genes meeting the following criteria were selected for pseudotime analysis using the "Monocle" package: genes had to be expressed in more than 10 cells, with a mean expression value greater than 0.5, a q value of differential expression analysis less than 0.01, and a dispersion value greater than or equal to the expected value. Subsequently, the "reduceDimension" function was applied to reduce the multidimensional space of cells to a two-dimensional space, and individual cells were sorted. Pseudotime analysis can reveal the differentiation relationship between cell types.

2.3. Analysis of Bulk RNA-Seq Data Set. *2.3.1. Identification of DEGs and Pathways Enrichment Analysis.* The "limma" package was utilized to analyze the DEGs between the VA-ECMO success group and failure group in the bulk RNA-seq data set. DEGs with $\log 2\ FC > 1$ and $P < 0.05$ were considered significantly upregulated, while those with $\log 2\ FC < -1$ and $P < 0.05$ were deemed significantly downregulated. These DEGs were visualized using a heatmap and a volcano plot. Subsequently, pathway enrichment analysis of the DEGs was conducted, encompassing Kyoto Encyclopedia of genes and genomes (KEGG) and gene set enrichment analysis (GSEA), with an adjusted $P < 0.05$ indicating significant enriched pathways.

2.3.2. Immune Infiltration Analysis. The CIBERSORT algorithm was utilized to quantify the infiltration levels of 22 different immune cells in the transcriptome data. The Wilcox test was employed to compare the differences in immune infiltration levels between the VA-ECMO success and failure groups, and these differences were visualized using the "vioplot" package. Subsequently, correlations among different immune cells were evaluated using the "Corrplot" package.

2.3.3. Identification of Genes Associated with the Prognosis of VA-ECMO. The following DEGs were intersected and are presented as a Venn diagram: DEGs between the VA-ECMO success group and failure group in the bulk RNA-seq data set, DEGs between the death group and survival group at 72 h after VA-ECMO establishment in the subset of NK/NKT cells of the scRNA-seq data set, and DEGs between the death group and survival group at 72 h after VA-ECMO establishment in the subset of B cells of the scRNA-seq data set. Genes associated with the ECMO prognosis could be identified after this intersection.

Next, we compared the expression differences of genes related to VA-ECMO prognosis between the ECMO success group and

https://doi.org/10.1021/acsomega.4c07339
ACS Omega 2025, 10, 637−654

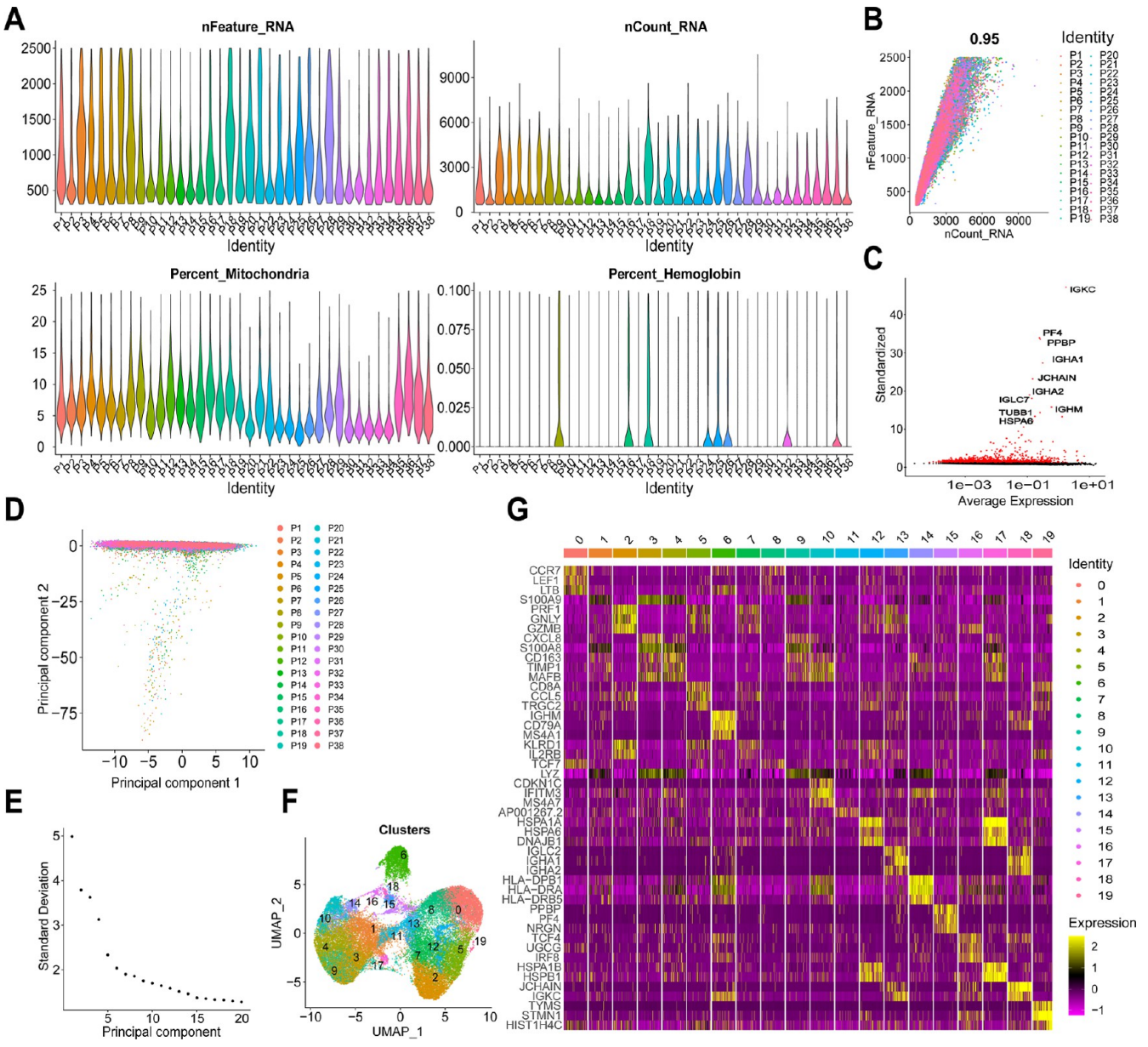

Figure 1. Processing of single-cell sequencing data. (A) nFeature_RNA, nCount_RNA, proportion of mitochondrial genes, and proportion of erythrocyte genes for each sample. (B) Correlation between nFeature_RNA and nCount_RNA of cells. (C) The volcano plot depicted the cellular HVGs at the cellular level (red colored dots), with the top 10 HVGs clearly labeled. (D) PCA demonstrated no significant batch effect among the 38 samples. (E) The number of PCs was determined as 10 using "ElbowPlot" function. (F) A UMAP visualization displayed 20 cell clusterings of PBMCs, with different cell clusters represented in various colors. (G) The heatmap depicted the top 3 DEGs, marked in yellow, within each cell clustering.

failure group in the transcriptome data set. The "pROC" package was utilized to generate the receiver operating characteristic (ROC) curve for evaluating the efficacy of genes associated with ECMO prognosis in predicting ECMO outcomes.

2.4. Experimental Validation of Genes Associated with the Prognosis of VA-ECMO. *2.4.1. Collection of Clinical Samples and Data.* Peripheral blood samples were collected from patients with CS receiving VA-ECMO support prior to ECMO establishment from March 2024 to July 2024. Anticoagulant tubes were used for the collection of peripheral blood samples, and PBMCs were separated and extracted using Ficoll lymphocyte separation solution (TBD, Tianjin, China) within 4 h of collection. The isolated PBMCs were then divided into frozen storage tubes, placed in a programmed cooling box, and stored at −80 °C for subsequent experiments involving real-time fluorescent quantitative PCR (RT-PCR) and western blot (WB). A total of 12 patients were included in the study, with 6 patients grouped into the VA-ECMO success group and another 6 patients in the VA-ECMO failure group. The VA-ECMO success group was defined as those who successfully weaned from ECMO and survived more than 7 days after weaning. Conversely, the VA-ECMO failure group consisted of patients who either failed to wean from ECMO or died within 7 days after ECMO establishment. All procedures performed in studies involving human participants were in accordance with the 1964 Helsinki Declaration. The study was approved by the Bioethics Committee of the Union Hospital of Fujian Medical University (2024KY244). All patients or their families provided informed consent to participate in the study.

https://doi.org/10.1021/acsomega.4c07339
ACS Omega 2025, 10, 637−654

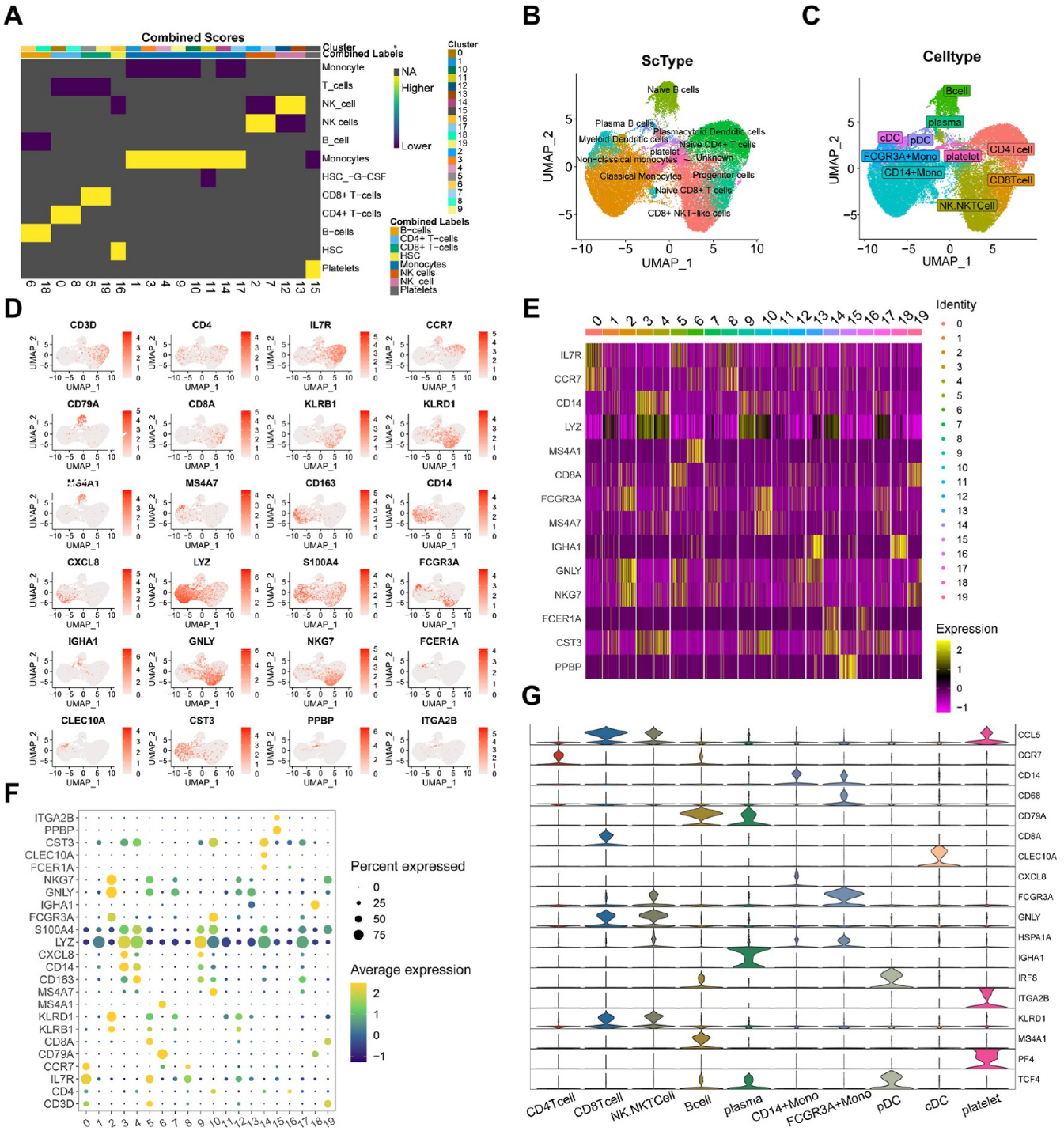

Figure 2. Annotation of the cell clusterings. (A) The cell clusterings were annotated using the "SingleR" package. The abscissa represented the cell clusterings, while the ordinate represented the cell types. The yellow color indicated the cell types corresponding to the clusterings. (B) Cell clusterings were annotated using the "Sc-Type" method. (C) The UMAP plot displayed 10 cell types based on the DEGs, along with annotation of the cell clusterings by Cellmarker's online webpage as well as annotation results from the "SingleR" package and "Sc-Type" method. Different cell types were depicted in different colors. (D) FeaturePlot diagrams illustrated the expression distribution of marker genes in cell clusterings. (E) DoHeatmap diagrams displayed expression of marker genes in cell clusterings. (F) DotPlot diagrams showed the expression of marker genes in cell clusterings. (G) VlnPlot diagrams exhibited the expression of marker genes in different cell types.

2.4.2. Real-Time Fluorescent Quantitative PCR (RT-PCR). The RT-PCR experiment was conducted to compare the mRNA levels of the genes associated with VA-ECMO prognosis between the ECMO success and failure groups. Total mRNA from PBMCs was extracted using the RNAeasyPlus Animal RNA Extraction kit (Beyotime, China), and the RNA concentration was measured using a spectrophotometer. Reverse transcription was carried out using the PrimeScript RT Master Mix Kit (Takara, Japan), followed by quantitative PCR amplification using TB Green Premix Ex *Taq*II (Takara, Japan). β-Actin served as the reference gene. The primer sequence for human HSPA1B was as follows:

https://doi.org/10.1021/acsomega.4c07339
ACS Omega 2025, 10, 637−654

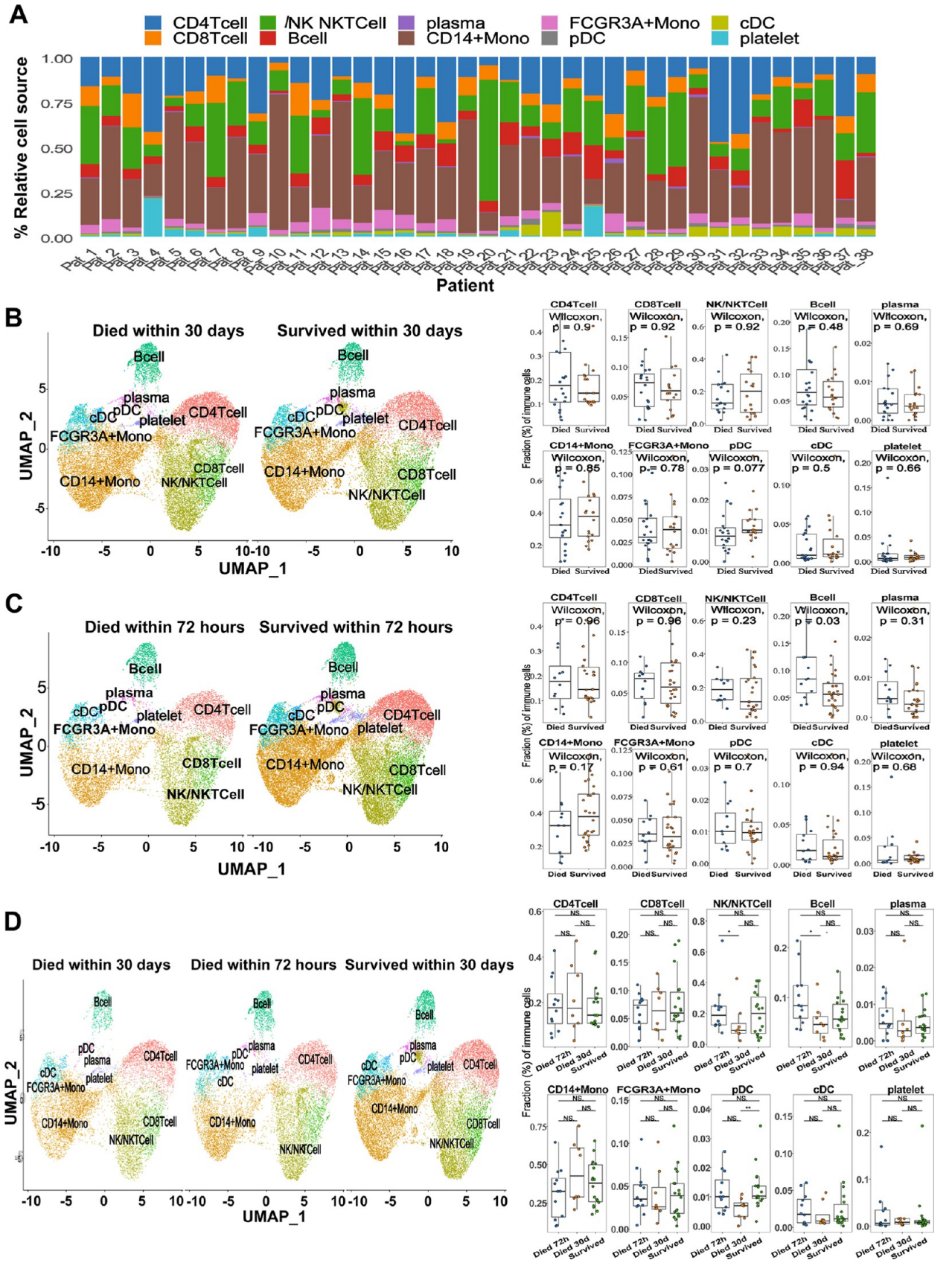

Figure 3. Comparison of the proportions of different cell types in groups with different VA-ECMO prognoses. (A) The bar graphs illustrate the distribution of proportions of each cell type for every VA-ECMO patient. (B) UMAP plots of different cell types and the comparison of proportions of different cell types between the 30-day death group and the 30-day survival group. (C) UMAP plots of different cell types and the comparison of proportions of different cell types between the 72-h death group and the 72-h survival group. (D) UMAP plots of different cell types and the comparison of proportions of different cell types among the early death group, the late-death group, and the 30-day survival group.

https://doi.org/10.1021/acsomega.4c07339
ACS Omega 2025, 10, 637−654

Forward: 5′-GCGAGGCGGACAAGAAGAAA-3′;
Reverse: 5′-GATGGGGTTACACACCTGCT-3′. All PCR samples were quantified using the comparative CT method to obtain relative expression levels, and the mRNA levels of the genes related to the VA-ECMO prognosis were compared between different prognostic groups.

2.4.3. Western Blot. Total proteins from PBMCs were extracted using a phosphoprotein extraction kit (KGI Bio, China). The protein concentration was determined using a BCA Protein Concentration Assay kit (Beyotime, China). After being denaturated with heat, the total proteins were separated by SDS-PAGE and transferred to PVDF membranes by electrophoresis. The PVDF membrane was blocked with fast blocking solution (Beyotime, China) for 15 min, followed by three washes with TBST for 10 min each time. Subsequently, the PVDF membrane with proteins was incubated with primary antibodies overnight at 4 °C and then washed again with TBST for 10 min three times the next day. The membranes were then incubated with a secondary antibody for 1 h at room temperature and washed again with TBST for 10 min three times. WB images were obtained using an ECL chemiluminescence allergic chromogenic reagent kit (YESEN creatures, China) and a chemical luminescence gel imaging system (Bole ChemiDocTM, America). β-Actin served as the reference gene. The primary antibody used was rabbit anti-HSP70 antibody (Bioss, China; #bs-0126R), and the secondary antibody was antirabbit IgG, HRP-linked antibody (Cell Signaling Technology, USA; #7074).

2.5. Statistical Analysis. R language (ver. 4.2.0) and Graphpad Prism software (ver. 9.5.0) were employed for the statistical analysis. The Wilcoxon test was utilized for comparison between two groups, while the Kruskal−Wallis test was used for comparison among three or more groups. Correlation coefficients between two continuous variables were calculated by using the Spearman method. Additionally, an ROC curve was generated to assess the prognostic value of genes related to the VA-ECMO prognosis. A significance level of $P < 0.05$ was considered to indicate statistically significant differences.

3. RESULTS

3.1. Data Set Information. A search of the GEO database revealed two data sets related to the clinical outcomes of VA-ECMO: the scRNA-seq data set (GSE127221) and the bulk RNA-seq data set (GSE93101). Samples for sequencing in both data sets were PBMCs from VA-ECMO patients collected before ECMO establishment. The sequencing platform of the GSE127221 data set was GPL24676 Illumina NovaSeq 6000 (*Homo sapiens*, USA). This data set contains 38 patients with acute heart failure (including acute exacerbation of chronic heart failure) who received VA-ECMO support. PBMC samples were collected from patients at the time of ECMO intubation (±79 min). Twelve patients who died within 72 h after ECMO establishment were grouped as the early death group, while eight patients who survived at 72 h after ECMO establishment but died late at 30 days were grouped as the late-death group. A total of 20 patients died within 30 days and were grouped together as the dead group, while the remaining 18 patients who survived after 30 days were grouped as the survival group. On the other hand, the sequencing platform of GSE93101 data set was GPL14951 Illumina Human HT-12 WG-DASL V4.0 R2 expression beadchip. The GSE93101 data set contains 34 cases of patients with CS, with 17 patients in the VA-ECMO success group and another 17 patients in the VA-ECMO failure group. The success group was defined as those surviving for more than 7 days after ECMO establishment, whereas those who died or developed multiple organ failure within 7 days after ECMO establishment comprised the failure group.

3.2. Processing of scRNA-Seq Data. A total of 61,764 cells from the scRNA-seq data set (GSE127221) were analyzed, and 32,425 genes were detected per cell. The raw data were rigorously preprocessed, quality controlled, and standardized. After genes and cells were filtered according to the set threshold, a total of 43,120 cells were retained. The gene expression signature of each sample is depicted in Figure 1A. A positive correlation was observed between nCount_RNA and nFeature_RNA of cells with a correlation coefficient of 0.95, indicating the good quality of the filtered cells (Figure 1B). The top 2000 HVGs of the cells were screened and displayed in a volcano plot, with IGKC, PPBP, PF4, IGHA1, JCHAIN, IGHA2, IGLC7, IGHM, TUBB1, and HSPA6 being identified as the top 10 HVGs (Figure 1C). PCA showed no significant batch effect among the 38 samples (Figure 1D), and then, a PC of 10 was selected for subsequent analysis (Figure 1E). Twenty cell clusterings were identified using 10 PCs, and the uniform manifold approximation and projection (UMAP) plot is shown in Figure 1F. Additionally, the top three DEGs for each cell clustering were listed in a heatmap (Figure 1G).

3.3. Annotation of the Cell Clusterings. The results of the automatic annotation of cell clusterings are presented in Figure 2A,B. Furthermore, based on the DEGs of cell clusterings and the annotation provided by the online webpage Cellmarker, a total of 10 cell types were comprehensively identified: B cells (2998 cells, 6.95%), CD4+ T cells (8063 cells, 18.7%), CD8+ T cells (3300 cells, 7.65%), CD14+ Monocytes (15,614 cells, 36.21%), FCGR3A+ Monocytes (1769 cells, 4.1%), NK/NKT cells (9127 cells, 21.17%), cDCs (823 cells, 1.91%), pDCs (478 cells, 1.11%), plasma cells (219 cells, 0.51%), and platelets (729 cells, 1.69%). The UMAP plot for these cell types is shown in Figure 2C. FeaturePlot diagrams displayed the expression distribution of marker genes in all the individual cells (Figure 2D). DoHeatmap and DotPlot diagrams depicted the expression of marker genes in the various cell clusterings, as shown in Figure 2E,F, respectively. A VlnPlot diagram illustrating the marker gene expression in cell types is also presented in Figure 2G.

3.4. Comparison of the Proportions of Different Cell Types in Groups with Different VA-ECMO Prognoses. The distribution of the proportions of each cell type for every patient is presented in Figure 3A, with the main cell types being CD14+ Monocytes, NK/NKT cells, and CD4 T cells. The distribution of cell types and the comparison of proportion of different cell types between the 30-day death group and the 30-day survival group are shown in Figure 3B. Additionally, the distribution of cell types and comparison of proportion of different cell types between the 72-h death group and the 72-h survival group are displayed in Figure 3C. Furthermore, the distribution of cell types and comparison of proportions of different cell types among the early death group (patients died within 72 h after VA-ECMO establishment), late-death group (patients survived at 72 h but died within 30 days after VA-ECMO establishment), and the 30-day survival group are illustrated in Figure 3D. The results indicated that there was no significant difference in the proportion of different cell types between the 30-day death group and the 30-day survival group. However, it is worth noting that B cells' proportion in the 72-h death group was significantly higher than those in the 72-h

https://doi.org/10.1021/acsomega.4c07339
ACS Omega 2025, 10, 637−654

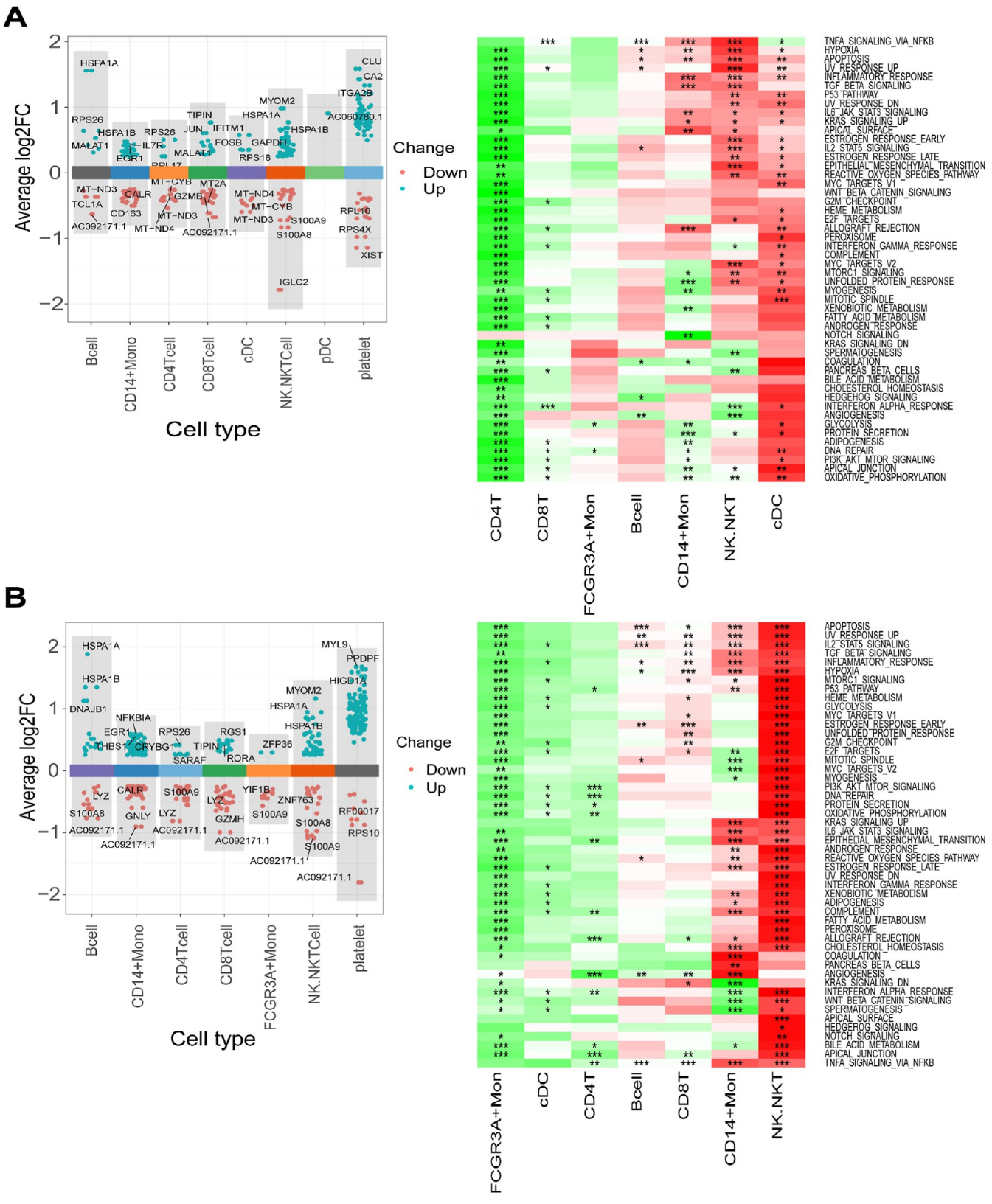

Figure 4. DEGs and their GSVA between groups with different VA-ECMO prognoses across different cell types. (A) The volcano plot illustrates the distribution of DEGs and their GSVA between the ECMO 30-day death group and the 30-day survival group in various cell types (30-day death group VS 30-day survival group). A redder color indicated a more pronounced upregulation of pathways, while a greener color indicated a more pronounced downregulation of pathways in GSVA. (B) The volcano plot depicts the distribution of DEGs and their GSVA between the ECMO 72-h death group and the 72-h survival group in different cell types (72-h death group vs 72-h survival group).

https://doi.org/10.1021/acsomega.4c07339
ACS Omega 2025, 10, 637−654

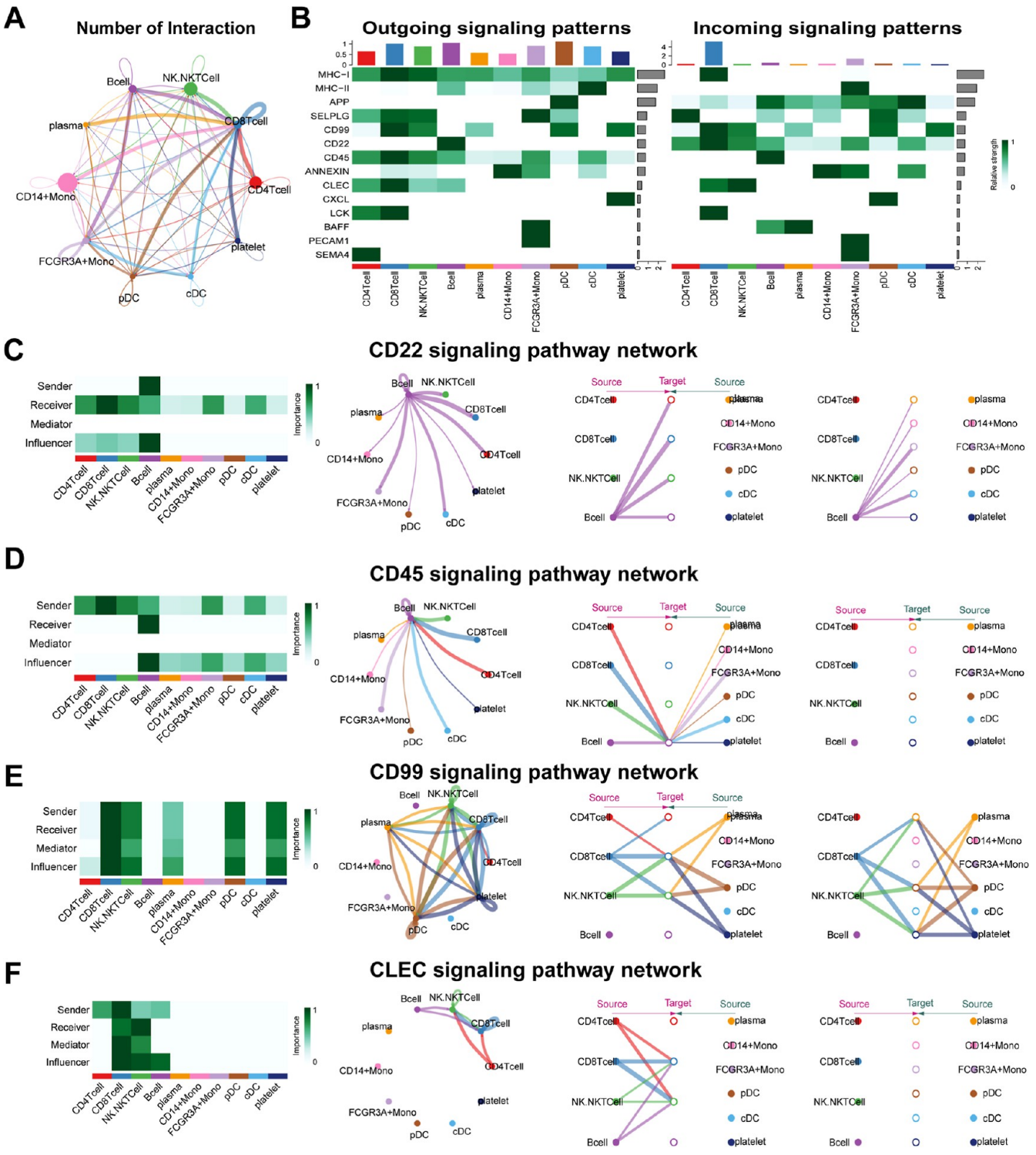

Figure 5. Cell−cell communication analysis. (A) The circular diagram depicts intercellular interactions among different cell types. The cells from which the arrows originate expressed the ligands, while the cells to which the arrows point expressed the receptors. The size of each dot represents the number of cells involved. (B) The heatmap illustrates common input and output signaling pathways shared among different cell types. (C) The heatmap, network map, and hierarchy map detail intercellular interactions within the CD22 signaling pathway. (D) The heat map, network map, and hierarchy map outline intercellular interactions within the CD45 signaling pathway. (E) The heat map, network map, and hierarchy map showcase intercellular interactions within the CD99 signaling pathway. (F) The heat map, network map, and hierarchy map display intercellular interactions in the CLEC signaling pathway.

survival group ($P < 0.05$). The analysis results of the three groups indicated that the proportion of NK/NKT cells and B cells in the early death group was significantly higher than that in the late-death group ($P < 0.05$) and pDC in the 30-day survival group was higher than that in the late-death group ($P < 0.05$). These findings suggested that changes in specific immune cell counts in peripheral blood before VA-ECMO establishment might serve as predictors for patient prognosis with VA-ECMO,

https://doi.org/10.1021/acsomega.4c07339
ACS Omega 2025, 10, 637−654

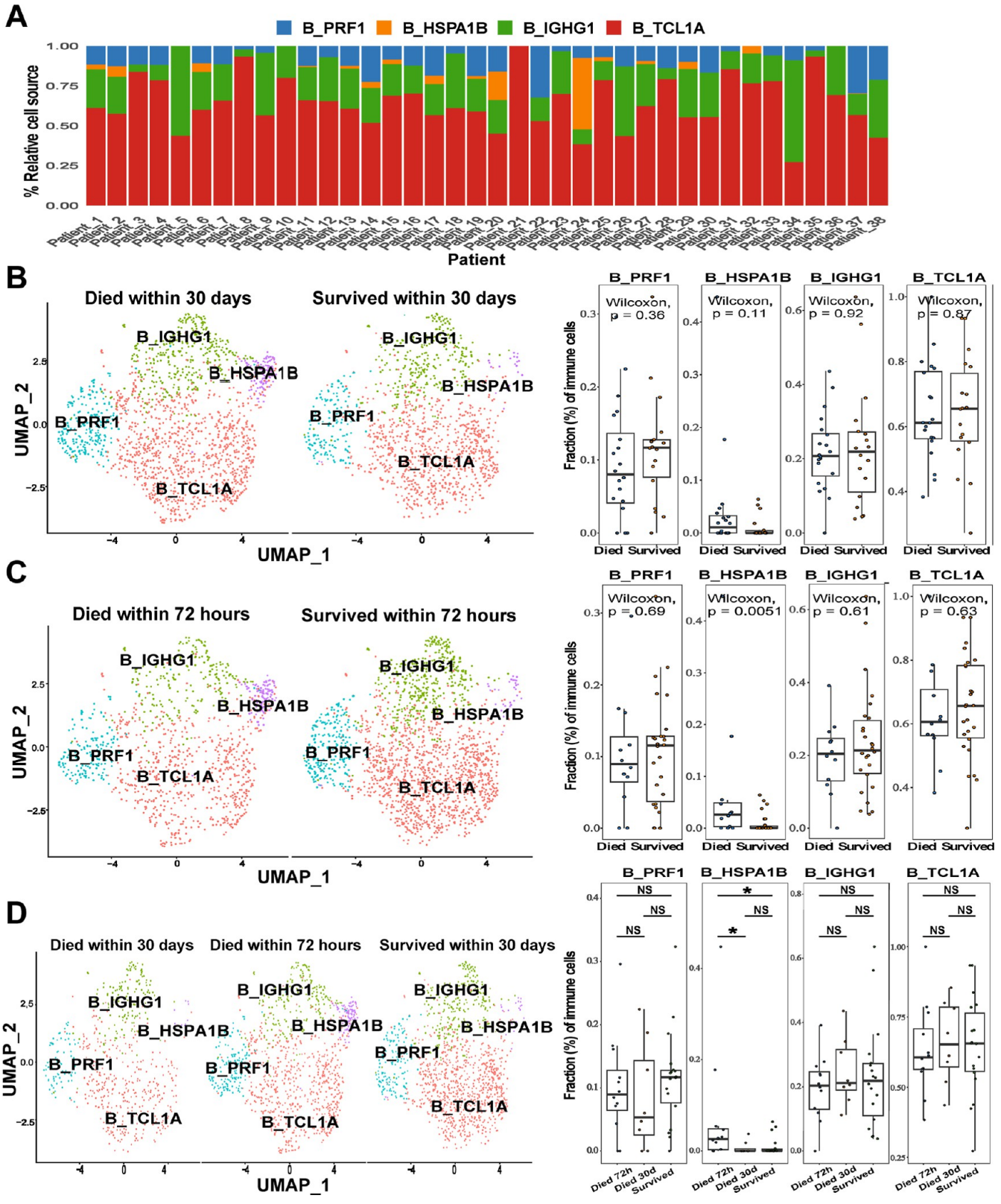

Figure 6. Comparison of the proportions of different B cell types in groups with different VA-ECMO prognoses. (A) The bar graphs illustrate the distribution of the proportions of each B cell type for every VA-ECMO patient. (B) UMAP plots of different B cell types and the comparison of proportions of different B cell types between the 30-day death group and the 30-day survival group. (C) UMAP plots of different B cell types and the comparison of proportions of different B cell types between the 72-h death group and the 72-h survival group. (D) UMAP plots of different B cell types and the comparison of proportions of different B cell types among the early death group, the late-death group, and the 30-day survival group.

and subsequently, clinical outcomes could potentially be improved by modulating specific immune cells. Due to a data set containing less than 500 pDC cells, further analysis of this cell type was avoided to prevent statistical bias. Additionally, DEGs

https://doi.org/10.1021/acsomega.4c07339
ACS Omega 2025, 10, 637−654

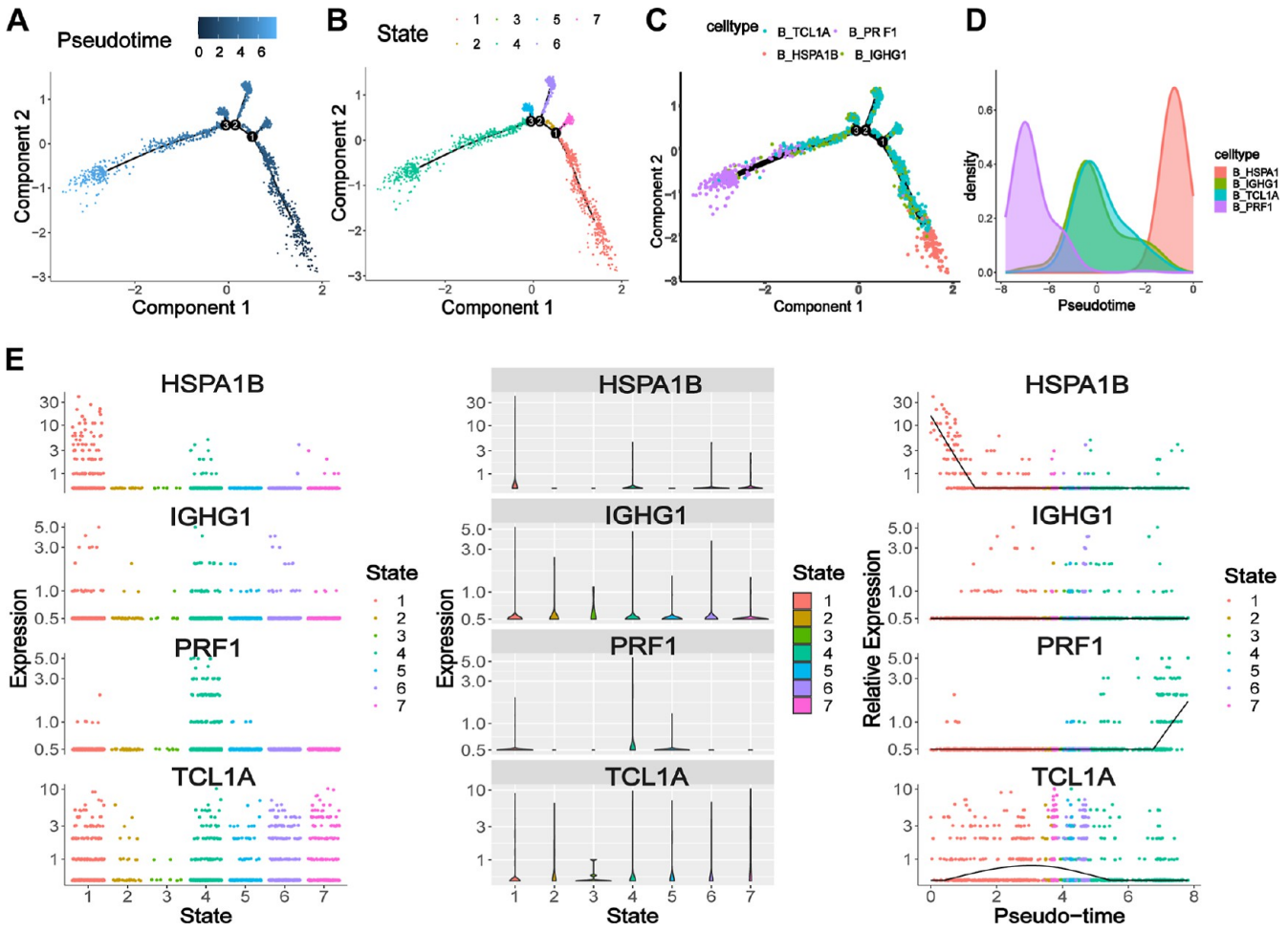

Figure 7. Pseudotime analysis of B cells in the death group. (A) Pseudotime trajectory plot of B cells depicts the order of dots from dark to light, representing the progression of pseudotiming. (B) Pseudotime trajectory plots illustrate different states of B cells. (C) Pseudotime trajectory plots showcase different types of B cells. (D) The diagram displays cell density along the time axis. (E) Expression changes of DEGs in the pseudotime trajectory.

of B cells and NK/NKT cells between different ECMO prognoses were further examined. It was speculated that B cells and NKT/NK cells might highly express certain prognosis-related genes, which could contribute to poor VA-ECMO prognosis.

3.5. DEGs and Their GSVA between Groups with Different VA-ECMO Prognoses across Different Cell Types. The DEGs and their GSVA between the ECMO 30-day death group and the 30-day survival group in different cell types are presented in Figure 4A. Similarly, the comparison between the 72-h death group and the 72-h survival group in different cell types is shown in Figure 4B. The findings indicated that DEGs associated with distinct ECMO prognoses were primarily linked to inflammatory response, tumorigenesis, cell proliferation and differentiation, as well as cell signal transduction. Notably, the expressions of HSPA1A and HSPA1B in B cells and NK/NKT cells were significantly higher in the death groups compared to those in the survival group ($P < 0.05$). Furthermore, B cells and NK/NKT cells exhibited significant enrichment and upregulation of pathways related to apoptosis, IL-2 signaling, STAT5 activation, inflammation, reactive oxygen species, and hypoxia in the death groups; conversely, these cell types showed downregulation in the angiogenesis pathway.

3.6. Cell−Cell Communication Analysis. The analysis of cell−cell communication revealed interactions between different cell types in PBMCs (Figure 5A). Additionally, the strength of the ligand−receptor interaction between different cell types is depicted in Figure 5B. It was evident that B cells exhibited significant ligand−receptor interactions with other cell types in both the CD22 and CD45 pathways (Figure 5C,D), while NK/NKT cells displayed distinct ligand−receptor interactions with other cell types in both the CD99 and c-type lectin structure domain (CLEC) pathways (Figure 5E,F). Given the significant upregulation of B cells and NK/NKT cells in the group with poor prognosis, as well as the noticeable ligand−receptor interactions across multiple pathways identified through cell−cell communication analysis in B cells and NK/NKT cells, further analyses on subsets for B cells and NK/NKT cells were warranted.

3.7. Subset of B Cells. *3.7.1. Processing of scRNA-Seq Data of B Cells and Cell Annotation of B Cell Clusterings.* After QC, a total of 2998 B cells were identified in the scRNA-seq data set. The top 2000 HVGs of the B cells were screened and visualized in a volcano plot, with the top 10 HVGs being HSPA1A, HSPA6, HSPA1B, DNAJB1, GNLY, HSPB1, HSP90AA1, IGHA2, IGLC3, and IGLV1−51 (Figure S1A). PCA revealed no significant batch effect among the 38 samples (Figure S1B), and a PC of 10 was selected for subsequent analysis (Figure S1C). Using these PCs to identify cell clusterings resulted in five distinct groupings, as shown in the

https://doi.org/10.1021/acsomega.4c07339
ACS Omega 2025, 10, 637−654

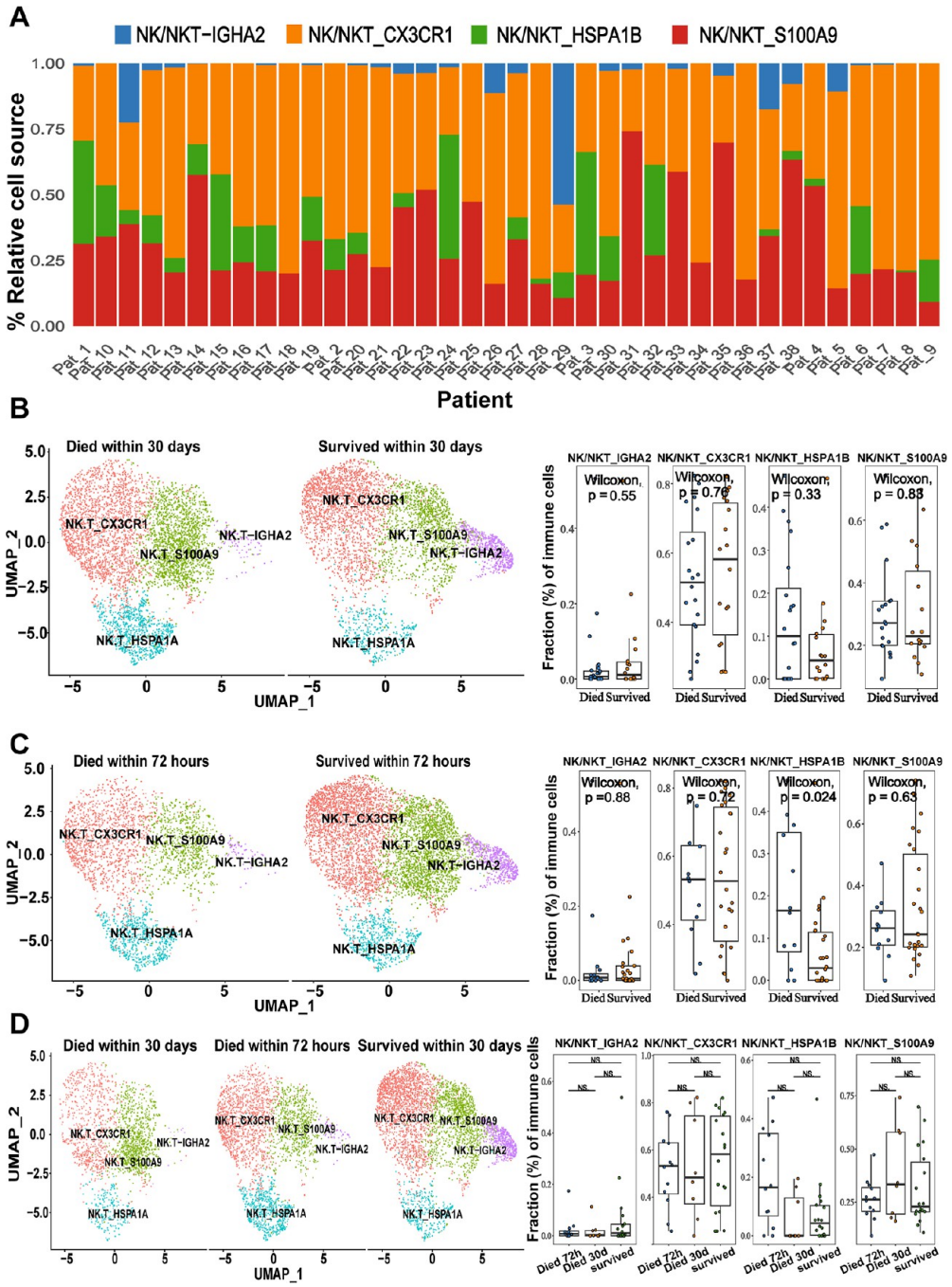

Figure 8. Comparison of the proportions of different NK/NKT cell types in groups with different VA-ECMO prognoses. (A) The bar graphs illustrate the distribution of the proportions of each NK/NKT cell type for every VA-ECMO patient. (B) UMAP plots of different NK/NKT cell types and the comparison of proportions of different NK/NKT cell types between the 30-day death group and the 30-day survival group. (C) UMAP plots of different NK/NKT cell types and the comparison of proportions of different NK/NKT cell types between the 72-h death group and the 72-h survival group. (D) UMAP plots of different NK/NKT cell types and the comparison of proportions of different NK/NKT cell types among the early death group, the late-death group, and the 30-day survival group.

UMAP plot (Figure S1D). Additionally, a heatmap displaying the top three DEGs for each B cell clustering was generated (Figure S1E). Based on these DEGs and annotation from the online webpage of Cellmarker for B cell clusterings, four distinct B cell types were identified: B-IGHG1 (597 cells, 12.7%), B-HSPA1B (140 cells, 4.7%), B-PRF1 (382 cells, 19.9%), and B-TCLIA (1879 cells, 62.7%), and their UMAP plot is displayed in Figure S1F. Furthermore, FeaturePlot diagrams illustrating the expression distribution of marker genes in B cells are presented in Figure S1G.

3.7.2. Comparison of the Proportions of Different B Cell Types in Groups with Different VA-ECMO Prognoses. The distribution of the proportions of each B cell type for every patient is depicted in Figure 6A, with the predominant cell types being B-TCL1A cells. The distribution of B cell types and the comparison of the proportion of different B cell types between the 30-day death group and the 30-day survival group are

https://doi.org/10.1021/acsomega.4c07339
ACS Omega 2025, 10, 637−654

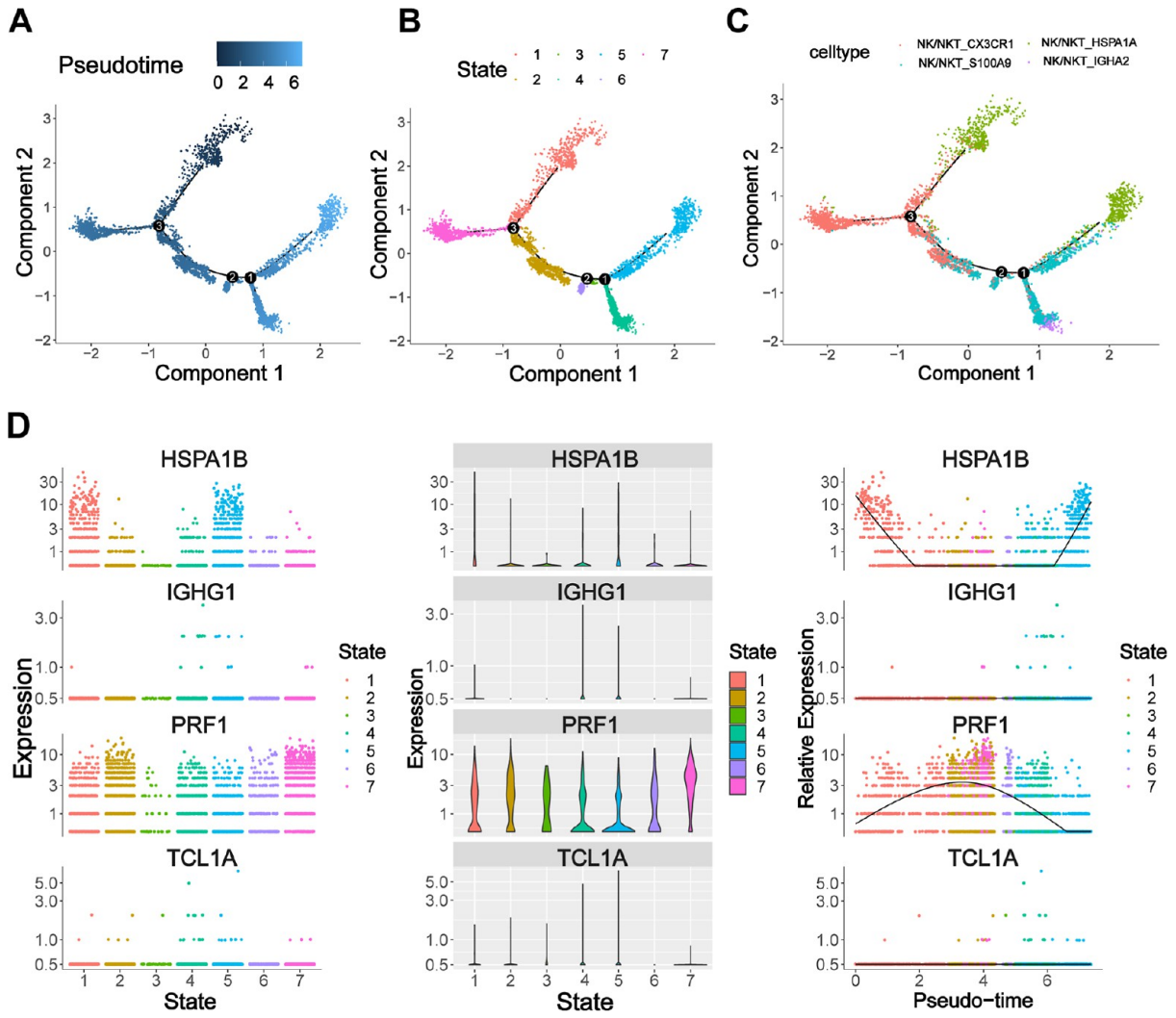

Figure 9. Pseudotime analysis of NK/NKT cells in the death group. (A) Pseudotime trajectory plots of NK/NKT cells depict the order of dots from dark to light, representing the progression of pseudotiming. (B) Pseudotime trajectory plots illustrate different states of NK/NKT cells. (C) Pseudotime trajectory plots showcase different types of NK/NKT cells. (D) Expression changes of DEGs in the pseudotime trajectory.

illustrated in Figure 6B. Additionally, the distribution of B cell types and comparison of proportion of different B cell types between the 72-h death group and the 72-h survival group are presented in Figure 6C. Furthermore, Figure 6D displays the distribution of cell types and comparison of proportion of different B cell types among the early death group, late-death group, and 30-day survival group. The findings indicated that there was no significant difference in the proportion of different B cell types between the 30 day death group and the 30 day survival group. However, it was observed that there was a significantly higher proportion of B-HSPA1B cells in the 72-h death group compared to those in the 72-h survival group ($P < 0.05$). Moreover, analysis revealed that there was a significantly higher proportion of B-HSPA1B cells in the early death group than in the late-death group among the comparison of three groups ($P < 0.05$). These results suggested that high expression levels of HSPA1B in B cells might be associated with poor prognosis for ECMO patients.

3.7.3. Pseudotime Analysis of B Cells in the Death Group. A pseudotime analysis was conducted on B cells in the VA-ECMO death group, and the evolutionary trajectories of B cells are depicted in Figure 7A−E. The analysis indicated that B-PRF1 represented the earliest differentiated B cell cohort, followed by a gradual transformation into B-HSPA1B. Consequently, an increased presence of B-HSPA1B cells might serve as a potential predictor for adverse outcomes in VA-ECMO patients.

3.8. Subset of NK/NKT Cells. *3.8.1. Processing of scRNA-Seq Data of NK/NKT Cells and Cell Annotation of NK/NKT Cell Clusterings.* After QC, a total of 9127 NK/NKT cells were identified in the scRNA-seq data set. The top 2000 HVGs of the NK/NKT cells were selected and visualized in a volcano plot, with the top 10 HVGs being HSPA6, HSPA1A, IGKC, DNAJB1, HSPA1B, HSP90AA1, CCL4L2, SERPINH1, HSPB1, and PTGDS (Figure S2A). PCA revealed no significant batch effect among the 38 samples (Figure S2B), and subsequently, a PC of 10 was chosen for further analysis (Figure S2C). Utilizing 10 PCs resulted in the identification of five distinct cell clusterings, as depicted in the UMAP plot in Figure S2D. Additionally, a heatmap displaying the top three DEGs for each NK/NKT cell clustering was generated (Figure S2E). Based on these DEGs and annotation from the online webpage of Cellmarker for NK/NKT cell clusterings, four distinct types of NK/NKT cells were characterized: NK/NKT-IGHA2 (671 cells, 7.35%), NK/NKT-CX3CR1 (4192 cells, 45.93%), NK/NKT-HSPA1B (1153 cells, 12.63%), and NK/NKT-S100A9 (3111 cells, 34.09%). Their UMAP plot is displayed in Figure

https://doi.org/10.1021/acsomega.4c07339
ACS Omega 2025, 10, 637−654

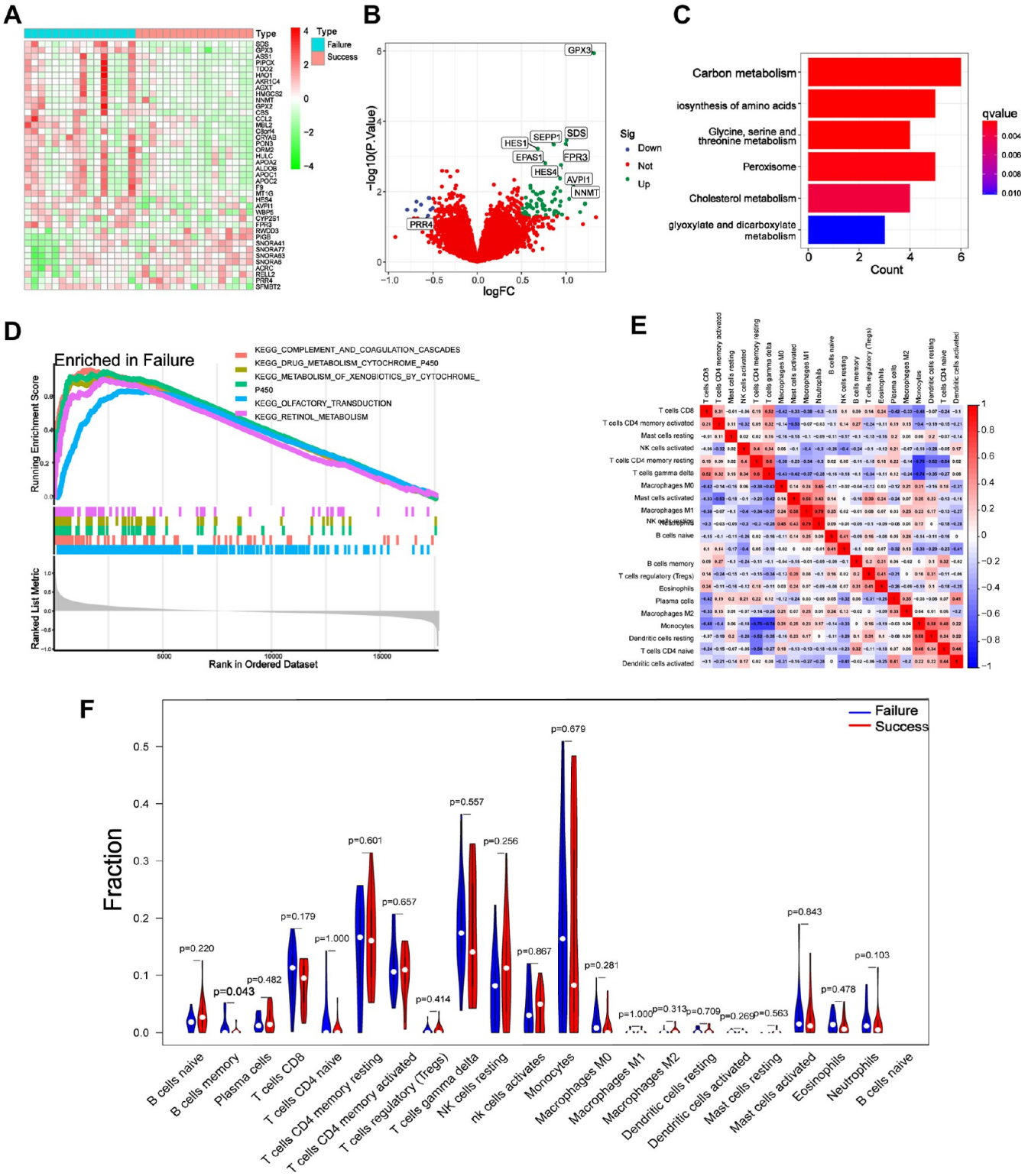

Figure 10. DEGs, pathway enrichment analysis, and immune cell infiltration analysis between ECMO success and failure groups. (A) The heatmap displays the top 20 upregulated or downregulated genes in the ECMO success and failure groups. (B) The volcano plot illustrates the DEGs in the ECMO success and failure groups, with a log FC > 0.5 and $P < 0.05$ (failure group vs success group). (C) KEGG analysis of DEGs between the ECMO success and failure groups. (D) GSEA conducted in the ECMO failure group. (E) Correlation analysis between different immune cells. (F) Immune cell infiltration analysis between the ECMO success and failure groups.

S2F. Furthermore, a DotPlot diagram illustrating the expression distribution of marker genes in NK/NKT cells is presented in Figure S2G.

3.8.2. Comparison of the Proportions of Different NK/NKT Cell Types in Groups with Different VA-ECMO Prognoses. The distribution of the proportions of each NK/NKT cell type for every patient is depicted in Figure 8A, with the predominant cell

https://doi.org/10.1021/acsomega.4c07339
ACS Omega 2025, 10, 637−654

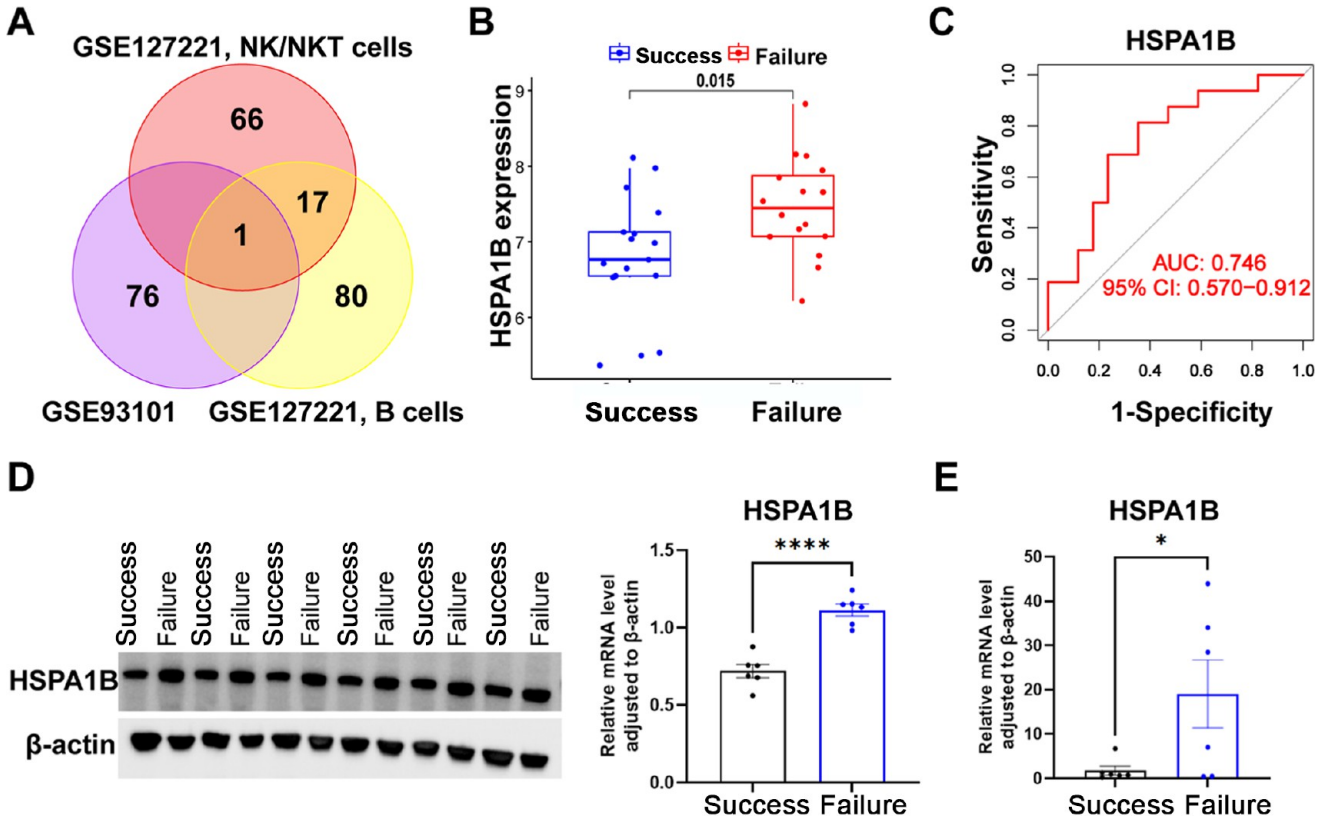

Figure 11. Experimental validation at the clinical level of DEGs at the intersection of scRNA-seq and bulk RNA-seq data set. (A) The Venn diagram illustrates the intersection of DEGs between groups with different prognoses of VA-ECMO in both the bulk-RNA data set and the scRNA-seq data set. (B) Analysis of HSPA1B mRNA levels between the ECMO success and failure groups in the bulk RNA-seq data set. (C) The ROC curve was utilized to assess the predictive efficacy of HSPA1B for ECMO prognosis. (D) Comparison of protein levels of HSPA1B in PBMCs collected before ECMO establishment between ECMO success and failure groups. (E) Comparison of mRNA levels of HSPA1B in PBMCs collected before ECMO establishment between ECMO success and failure groups.

types being NK/NKT-CX3CR1 cells. The distribution of NK/NKT cell types and the comparison of proportion of different NK/NKT cell types between the 30-day death group and the 30-day survival group are illustrated in Figure 8B. Similarly, the distribution of NK/NKT cell types and comparison of proportion of different NK/NKT cell types between the 72-h death group and the 72-h survival group are presented in Figure 8C. Furthermore, Figure 8D displays the distribution of cell types and a comparison of proportion of different NK/NKT cell types among the early death group, late-death group, and 30-day survival group. The results indicated that there was no significant difference in the proportion of different NK/NKT cell types between the 30-day death group and the 30-day survival group. Additionally, there was no significant difference in proportion of different NK/NKT cell types among these three groups. However, it was noteworthy that the proportion of NK/NKT-HSPA1B cells in the 72-h death group was significantly higher than those in the 72-h survival group ($P < 0.05$), suggesting that NK/NKT cells with high HSPA1B expression might lead to poor prognosis of ECMO.

3.8.3. Pseudotime Analysis of NK/NKT Cells in the Death Group. A pseudotime analysis was conducted to assess the NK/NKT cells in the VA-ECMO death group. The evolutionary trajectories of NK/NKT cells are depicted in Figure 9A−D, revealing that these cells might originate from NK/NKT-HSPA1B cells, experiencing a subsequent decrease, and then gradually increased again. Consequently, the elevated presence of NK/NKT-HSPA1B cells could potentially serve as an indicator for a poorer prognosis in VA-ECMO patients.

3.9. Analysis of the Bulk RNA-Seq Data Set. The ECMO prognosis-related transcriptome data set (GSE93101) comprised 34 patients with CS who received VA-ECMO support. The ECMO success group ($n = 17$) was defined as those patients who survived for more than 7 days after the establishment of ECMO, while the ECMO failure group ($n = 17$) was defined as those patients who died or experienced multiorgan failure within 7 days after the establishment of ECMO.

3.9.1. Identification of DEGs, Pathway Enrichment Analysis, and Immune Cell Infiltration Analysis between the ECMO Success and Failure Group. The heatmap and volcano plot of DEGs in the ECMO success versus failure group are depicted in Figure 10A,B. The KEGG and GSEA analyses of DEGs are presented in Figure 10C,D. The DEGs were primarily enriched in pathways related to carbon metabolism, biosynthesis of amino acids, glycine, serine and threonine metabolism, cholesterol metabolism, and glyoxylate and dicarboxylate metabolism. In contrast, the failure group was predominantly associated with pathways involving complement and coagulation cascades, drug metabolism by cytochrome P450, and metabolism of xenobiotics by cytochrome P450. The correlation analysis between different immune cells is illustrated in Figure 10E, demonstrating a strong correlation between NK cell resting and B cell native. This finding aligned with the results of cell−cell communication analysis from the scRNA-seq data set indicating interaction between NK cells and B cells. Addition-

https://doi.org/10.1021/acsomega.4c07339
ACS Omega 2025, 10, 637−654

ally, the comparison of immune cell infiltration between ECMO success and failure group is shown in Figure 10F. It revealed that memory B cell infiltration was significantly higher in the failure group compared to the success group, consistent with findings from the scRNA-seq data set analysis. Notably, there was no difference observed in NK/NKT cell infiltration between the success and failure groups. This inconsistency might be attributed to combined analysis of NK and NKT cells within the scRNA-seq data set, which might affect the results.

3.9.2. Experimental Validation at the Clinical Level of the DEGs Identified at the Intersection of scRNA-Seq Data Set and Bulk RNA-Seq Data Set. The intersection of the following DEGs was taken: DEGs between the ECMO success and failure groups in the bulk-RNA data set, DEGs between the ECMO 72-h death group and survival group in the NK/NKT cells of the scRNA-seq data set, and DEGs between the ECMO 72-h death group and survival group in the B cells of the scRNA-seq data set. The result was presented as a Venn diagram (Figure 11A), which indicated that HSPA1B, an upregulated gene (Log FC > 0.5, $P < 0.05$), was a common DEG among all three groups. These findings suggested that HSPA1B might serve as a key predictor of ECMO outcome. Furthermore, levels of HSPA1B mRNA were significantly higher in the ECMO failure group compared to the success group in transcriptome data ($P < 0.05$, Figure 11B). The ROC curve analysis demonstrated that HSPA1B had a better prognostic predictive efficiency for patients receiving VA-ECMO (Figure 11C).

Among the 12 clinical patients, the indication for receiving VA-ECMO was either low cardiac output syndrome following cardiac surgery or the acute onset of chronic heart failure. Both the success group and the failure group consisted of 66.7% males, with an average age of (56.6 ± 18.5) years old and (58.2 ± 13.8) years old, respectively. The ECMO running time was (93.3 ± 16.6) hours and (80.2 ± 104.0) hours, respectively. The comparison of protein and mRNA levels of HSPA1B in the PBMCs collected from patients before ECMO establishment, between the ECMO success and failure groups, is illustrated in Figure 11D,E.

4. DISCUSSION

In this study, two data sets related to the prognosis of VA-ECMO were analyzed. The analysis of the scRNA-seq data set revealed that the proportion of B cells and NK/NKT cells in PBMCs collected before VA-ECMO establishment was significantly higher in patients with poor prognoses of VA-ECMO compared to those with better outcomes. Therefore, it was speculated that the counts of circulatory immune cells before VA-ECMO establishment might predict the prognosis of patients with CS receiving VA-ECMO support. The upregulated expression of HSPA1B in B cells and NK/NKT cells as well as in total PBMCs before VA-ECMO establishment might serve as markers for a poor prognosis of VA-ECMO.

However, there is limited research on the functional status of immune cells in peripheral blood before VA-ECMO establishment and their relationship to the prognosis of VA-ECMO. Biomarkers in PBMCs have been shown to predict the prognosis of certain diseases. For instance, a study by professors Sabine Bahn and Jakub Tomasik from the University of Cambridge in the United Kingdom revealed that patients with schizophrenia exhibit three PBMC biomarkers, including CD36 and insulin receptor on helper T cells' surface, as well as monocyte surface glucose transporter 1, which can serve as objective physiological indicators for diagnosing schizophrenia and distinguishing it from other mental disorders.[5] Al-Aly et al. confirmed through epidemiological studies that an increased number of peripheral blood monocytes was associated with new-onset CKD, CKD progression, and CKD-related mortality.[6] Additionally, Kreuter M et al. found that monocyte counts in peripheral blood can predict the severity and prognosis of idiopathic interstitial fibrosis diseases, and higher absolute monocyte counts are significantly linked to shorter survival in patients with fibrotic diseases such as systemic sclerosis, myelofibrosis, and hypertrophic cardiomyopathy.[7]

In the current study, the observed increase in the level of B cells and NK/NKT cells in PMBCs was found to be associated with a poor prognosis in VA-ECMO patients with CS. B cells play a key role in specific humoral immunity as they are capable of secreting antibodies, various cytokines, and some chemokines to regulate immune responses. NK cells have the ability to not only eliminate tumor cells and virus-infected cells but also secrete a variety of cytokines. Furthermore, NK cells share a close developmental relationship with T cells. NKT cells are special T cells that express both the T cell receptor and NK cell receptor on their surfaces. During the process of scRNA-seq annotation, distinguishing between NK and NKT cells proved to be challenging. Therefore, in this study, NK cells and NKT cells were combined into the NK/NKT cell type. Changes in the counts of B and NK/NKT cells have been linked to certain diseases. For instance, patients with chronic obstructive pulmonary disease (COPD) exhibit increased counts of lung lymph follicles as well as elevated levels of serum B cell-activating factor of tumor necrosis factor family (BAFF), and there is a significant increase in BAFF expression levels within B-cells present in blood and bronchoalveolar lavage fluid.[8] The continuous expression of BAFF within B cells promotes their survival within the lungs and leads to an expansion of lymph follicles—ultimately contributing to the progression of COPD. Similarly, patients diagnosed with Parkinson's disease demonstrate significantly increased counts of NK cells within peripheral blood lymphocytes.[9] These findings aligned closely with our own study results, indicating an increase in both B cells and NK/NKT cells among VA-ECMO patients with poor prognoses.

In this study, pathway enrichment analysis of DEGs in B cells and NK/NKT cells between groups with varying ECMO prognoses revealed that DEGs played significant roles in pathways associated with inflammation and apoptosis. This suggested that patients in the group with a poor prognosis exhibited a heightened intensity of the inflammatory response. The analyses of scRNA-seq and bulk RNA-seq data sets indicated interactions between different immune cells, including B cells and NK/NKT cells. It was evident that B cells had substantial ligand−receptor interactions with other cell types in both the CD22 and CD45 signaling pathways, while NK/NKT cells exhibited significant ligand−receptor interactions with other cell types in both the CD99 and CLEC signaling pathways. Both CD22 and CD45 play crucial roles in cellular signal transduction, whereas CD99 and CLEC are involved in regulating the activity and function of NK/NKT cells. Furthermore, stimulation of inflammations or cytokines can lead to upregulated expression of CD99, which plays a role in cell adhesion, apoptosis, and signal transduction.[10] The CLEC signaling pathway is a signal transduction process mediated by CLEC receptors that is associated with biological functions, such as inflammation responses, immune surveillance, and intracellular interactions. Additionally, the expression of CLEC

https://doi.org/10.1021/acsomega.4c07339
ACS Omega 2025, 10, 637−654

is upregulated during infections.[11] Therefore, all of these pathways might be relevant to the activation of inflammatory responses. In summary, we speculated that VA-ECMO patients with upregulated B cells and NK/NKT cells associated with poor prognosis might be linked to strong inflammatory responses under stress as well as high expression levels of certain cytokines within these cell types.

This study demonstrated that high expression of HSPA1B in B cells and NK/NKT cells of PMBCs, as well as the increased expression level of HSPA1B in the total PMBCs collected before VA-ECMO establishment, were associated with poor prognosis. Pseudotime analysis also revealed that B cells and NK/NKT cells in the VA-ECMO death group gradually transformed into cells with a high expression of HSPA1B during cellular differentiation and development. Therefore, HSPA1B might serve as a predictor of the VA-ECMO prognosis. It is widely recognized that HSPA1B belongs to the heat shock protein 70 (HSP70) family. The HSP70 family consists of highly conserved peptides that are adaptively synthesized by cells under high temperature or exposure to harmful factors. The HSP70 gene exhibits polymorphism, including variants such as HSPA1A, HSPA1B, and HSPA1L. Functionally, HSP70 can inhibit protein misfolding and assist proteins in attaining their normal structure.[12] However, it may also play a dual role; moderate levels of its expression can protect cells from stress induced by injuries, while overexpression may lead to disease. For instance, it can stimulate monocytes to secrete proinflammatory factors such as IL-6, TNF-α, and IL-1.[13]

The expression of HSPs in most tumor tissues is significantly higher than that in nontumor tissues. For example, HSPs are overexpressed in human hepatocellular carcinoma (HCC) tissues and have been linked to the invasion and prognosis of HCC. Hepatitis B virus-related liver cancer promotes the proliferation of liver cancer cells, inhibits the apoptosis of liver cancer cells, and advances the progression of liver cancer through the axis of transcription factor 7-HSPA1B activated by microRNA-340-5p.[14] Overexpression of HSPA1B is associated with early metastasis and progression of bladder urothelial carcinoma,[15] ovarian cancer,[16] and cervical cancer.[17] Conversely, low expression levels of HSPA1A and HSPA1B are closely related to improved prognosis for colorectal cancer, suggesting their potential as prognostic biomarkers for this condition.[18] Furthermore, serum levels of HSP70 were found to be significantly elevated in patients with multiple sclerosis (MS) compared to healthy individuals.[19] Both HSPA1A and HSPA1B are upregulated in all brain regions of MS patients and may exacerbate the immune response associated with MS.[20] Additionally, it has been observed that HSPA1B is linked to noncognitive symptoms in late-onset Alzheimer's disease.[21] In a different context, both HSPA1A and HSPA1B show significant increases in blood samples from gout patients and are correlated to gout severity. This suggests their potential utility as diagnostic markers for gout.[22] Therefore, increased expression levels of HSPA1B in PBMCs can also serve as a prognostic marker for VA-ECMO. The heightened level may indicate excessive stress or inflammatory responses or could be attributed to its excessive release by B cells and NK/NKT cells.

HSP70 also plays a crucial role in circulatory diseases. The patients included in the data sets were primarily diagnosed with CS (acute heart failure or an acute exacerbation of chronic heart failure), so the upregulation of HSPA1B expression might also be associated with CS. It was found that HSP70 was significantly correlated with the decreasing left ventricular ejection fraction and the elevated NT-proBNP, suggesting its relevance to worsening cardiac function.[23] The severity of chronic heart failure was linked to HSP70 levels in the blood as well as to the HSPA1B polymorphism.[23] In the process of myocardial ischemia-reperfusion injury (IRI), HSP70 has a dual role. While it can play a protective role by regulating various intracellular proteins and signaling pathways, its overexpression can also activate proinflammatory pathways and aggravate IRI.[24] Additionally, extracellular HSP70 can activate the immune system, cause endothelial damage and atherosclerosis, and easily induce cardiac arrest.[25] It is speculated that HSPA1B may also be associated with myocardial IRI and cardiac arrest.[26] In this study, the upregulated HSPA1B possibly derived from B cells, NK/NKT cells, injured myocardium and internal organs, or necrotic/apoptotic cells before VA-ECMO establishment. The overexpression of HSPA1B might indicate excessive inflammatory and immune response, leading to poor prognosis. Most studies on VA-ECMO prediction models have shown that lactic acid level is related to prognosis in patients with CS undergoing VA-ECMO.[27] Increased lactic acid level is associated with microcirculation disorders and may also be linked to poor cardiac function, resulting in tissue hypoperfusion. Our analysis results aligned with previous outcome-related analyses.

There were certain limitations present in this article. First, a limited number of data sets were included in this study. Second, the definition of VA-ECMO prognosis differed between the scRNA-seq data set and bulk-RNA data set. Therefore, the results may be influenced by the inclusion bias. Third, B cells and NK/NKT cells exhibited significant differences in counts only between the early death group and the late-death group but not between the 30-day death group and the 30-day survival group. Consequently, further analysis of prognostic predictors for the long-term survival of VA-ECMO is warranted. Fourth, experimental validation in this study was confined to the transcriptome level, and further validation of PMBC counts and their marker genes are necessary.

5. CONCLUSIONS

The increased presence of B cells and NK/NKT cells in PBMCs was associated with a poor prognosis of VA-ECMO. High expression of HSPA1B in B cells, NK/NKT cells, and total PBMCs prior to the establishment of VA-ECMO were identified as a predictor of poor prognosis. Inhibiting the overexpression of HSPA1B in B cells or NK/NKT cells may potentially improve the outcome of VA-ECMO.

■ ASSOCIATED CONTENT

Data Availability Statement

The data utilized in this article were sourced from publicly available resources. The underlying data for this study can be accessed openly through the Gene Expression Omnibus database (https://www.ncbi.nlm.nih.gov/geo/), which includes data sets GSE127221 (https://www.ncbi.nlm.nih.gov/geo/query/acc.cgi?acc=GSE127221) and GSE93101 (https://www.ncbi.nlm.nih.gov/geo/query/acc.cgi?acc=GSE93101).

Supporting Information

The Supporting Information is available free of charge at https://pubs.acs.org/doi/10.1021/acsomega.4c07339.

Processing of scRNA-seq data of B cells and cell annotation of B cell clusterings and processing of scRNA-seq data of NK/NKT cells and cell annotation of NK/NKT cell clusterings (PDF)

https://doi.org/10.1021/acsomega.4c07339
ACS Omega 2025, 10, 637−654

AUTHOR INFORMATION

Corresponding Authors

Guodong Zhong − *Department of Pathology, Fujian Province Second People's Hospital, The Second Affiliated Hospital of Fujian University of Traditional Chinese Medicine, Fuzhou 350000, China*; Phone: 18459111686; Email: 18459111686@163.com

Liangwan Chen − *Department of Cardiovascular Surgery, Fujian Medical University Union Hospital, Fuzhou 350000, China; Key Laboratory of Cardio-Thoracic Surgery (Fujian Medical University) and Engineering Research Center of Tissue and Organ Regeneration, Fujian Province University, Fuzhou 350000, China*; orcid.org/0000-0002-8317-7412; Phone: 13358255333; Email: clw1259@163.com

Author

Lei Wang − *Department of Cardiovascular Surgery, Fujian Medical University Union Hospital, Fuzhou 350000, China; Key Laboratory of Cardio-Thoracic Surgery (Fujian Medical University), Fujian Province University, Fuzhou 350000, China*

Complete contact information is available at: https://pubs.acs.org/10.1021/acsomega.4c07339

Author Contributions

⊥G.Z. and L.C. contributed equally to this work.

Notes

The authors declare no competing financial interest.

ACKNOWLEDGMENTS

This study was funded by Joint Funds for the innovation of science and Technology, Fujian province (grant number: 2021Y9076), Fujian Provincial Natural Science Foundation of China (grant number: 2024J01644), and the National Natural Science Foundation of China (grant number: U2005202). We sincerely appreciate the financial support provided for this study.

REFERENCES

(1) Nunez, J. I.; Gosling, A. F.; O'Gara, B.; Kennedy, K. F.; Rycus, P.; Abrams, D.; Brodie, D.; Shaefi, S.; Garan, A. R.; Grandin, E. W. Bleeding and thrombotic events in adults supported with venovenous extracorporeal membrane oxygenation: an ELSO registry analysis. *Intensive Care Med.* **2022**, *48* (2), 213−224.

(2) Danial, P.; Olivier, M. E.; Bréchot, N.; Ponnaiah, M.; Schoell, T.; D'Alessandro, C.; Demondion, P.; Clément, M.; Juvin, C.; Carillion, A.; et al. Association between shock etiology and 5-year outcomes after venoarterial extracorporeal membrane oxygenation. *J. Am. Coll. Cardiol.* **2023**, *81* (9), 897−909.

(3) Ostadal, P.; Rokyta, R.; Karasek, J.; Kruger, A.; Vondrakova, D.; Janotka, M.; Naar, J.; Smalcova, J.; Hubatova, M.; Hromadka, M.; et al. Extracorporeal membrane oxygenation in the therapy of cardiogenic shock: results of the ECMO-CS randomized clinical trial. *Circulation* **2023**, *147* (6), 454−464.

(4) Ianevski, A.; Giri, A. K.; Aittokallio, T. Fully-automated and ultra-fast cell-type identification using specific marker combinations from single-cell transcriptomic data. *Nat. Commun.* **2022**, *13* (1), 1246.

(5) Zaki, J. K.; Lago, S. G.; Rustogi, N.; Gangadin, S. S.; Benacek, J.; van Rees, G. F.; Haenisch, F.; Broek, J. A.; Suarez-Pinilla, P.; Ruland, T.; et al. Diagnostic model development for schizophrenia based on peripheral blood mononuclear cell subtype-specific expression of metabolic markers. *Transl. Psychiatry* **2022**, *12* (1), 457.

(6) Bowe, B.; Xie, Y.; Xian, H.; Li, T.; Al-Aly, Z. Association between monocyte count and risk of incident CKD and progression to ESRD. *Clin. J. Am. Soc. Nephrol.* **2017**, *12*, 603−613.

(7) Kreuter, M.; Maher, T. M. Can monocytes predict prognosis of idiopathic pulmonary fibrosis? *Lancet Respir. Med.* **2019**, *7* (6), 467−469.

(8) Polverino, F.; Cosio, B. G.; Pons, J.; Laucho-Contreras, M.; Tejera, P.; Iglesias, A.; Rios, A.; Jahn, A.; Sauleda, J.; Divo, M.; et al. B Cell-activating factor. An orchestrator of lymphoid follicles in severe chronic obstructive pulmonary disease. *Am. J. Respir. Crit. Care Med.* **2015**, *192* (6), 695.

(9) Niwa, F.; Kuriyama, N.; Nakagawa, M.; Imanishi, J. Effects of peripheral lymphocyte subpopulations and the clinical correlation with Parkinson's disease. *Geriatr. Gerontol. Int.* **2012**, *12* (1), 102−107.

(10) van Wanrooij, E. J.; de Vos, P.; Bixel, M. G.; Vestweber, D.; van Berkel, T. J.; Kuiper, J. Vaccination against CD99 inhibits atherogenesis in low-density lipoprotein receptor-deficient mice. *Cardiovasc. Res.* **2008**, *78* (3), 590−596.

(11) Labed, S. A.; Wani, K. A.; Jagadeesan, S.; Hakkim, A.; Najibi, M.; Irazoqui, J. E. Intestinal epithelial Wnt signaling mediates acetylcholine-triggered host defense against infection. *Immunity* **2018**, *48* (5), 963−978.

(12) Zatsepina, O. G.; Evgen'ev, M. B.; Garbuz, D. G. Role of a heat shock transcription factor and the major heat shock protein Hsp70 in memory formation and neuroprotection. *Cells* **2021**, *10* (7), 1638.

(13) Asea, A.; Kraeft, S. K.; Kurt-Jones, E. A.; Stevenson, M. A.; Chen, L. B.; Finberg, R. W.; Koo, G. C.; Calderwood, S. K. HSP70 stimulates cytokine production through a CD14-dependant pathway, demonstrating its dual role as a chaperone and cytokine. *Nat. Med.* **2000**, *6*, 435−442.

(14) Song, F.; Wei, M.; Wang, J.; Liu, Y.; Guo, M.; Li, X.; Luo, J.; Zhou, J.; Wang, M.; Guo, D.; et al. Hepatitis B virus-regulated growth of liver cancer cells occurs through the microRNA-340−5p-activating transcription factor 7-heat shock protein A member 1B axis. *Cancer Sci.* **2019**, *110* (5), 1633−1643.

(15) Garg, M.; Kanojia, D.; Seth, A.; Kumar, R.; Gupta, A.; Surolia, A.; Suri, A. Heat-shock protein 70−2 (HSP70−2) expression in bladder urothelial carcinoma is associated with tumour progression and promotes migration and invasion. *Eur. J. Cancer* **2010**, *46*, 207−215.

(16) Gupta, N.; Jagadish, N.; Surolia, A.; Suri, A. Heat shock protein 70−2 (HSP70−2) a novel cancer testis antigen that promotes growth of ovarian cancer. *Am. J. Cancer Res.* **2017**, *7*, 1252−1269.

(17) Garg, M.; Kanojia, D.; Saini, S.; Suri, S.; Gupta, A.; Surolia, A.; Suri, A. Germ cell-specific heat shock protein 70−2 is expressed in cervical carcinoma and is involved in the growth, migration, and invasion of cervical cells. *Cancer* **2010**, *116*, 3785−3796.

(18) Jiang, W.; Pan, X.; Yan, H.; Wang, G. Prognostic Significance of the Hsp70 Gene Family in Colorectal Cancer. *Med. Sci. Monit.* **2021**, *27*, No. e928352.

(19) Lechner, P.; Buck, D.; Sick, L.; Hemmer, B.; Multhoff, G. Serum heat shock protein 70 levels as a biomarkerfor inflammatory processes in multiple sclerosis. *Mult. Scler. J. Exp. Transl. Clin.* **2018**, *4* (2), 2055217318767192.

(20) Chiricosta, L.; Gugliandolo, A.; Bramanti, P.; Mazzon, E. Could the Heat Shock Proteins 70 Family Members Exacerbate the Immune Response in Multiple Sclerosis? An in Silico Study. *Genes* **2020**, *11* (6), 615.

(21) Clarimón, J.; Bertranpetit, J.; Boada, M.; Tàrraga, L.; Comas, D. HSP70−2 (HSPA1B) is associated with noncognitive symptoms in late-onset Alzheimer's disease. *J. Geriatr. Psychiatry Neurol.* **2003**, *16* (3), 146−150.

(22) Li, Y.; Shan, C.; Yang, B.; Wang, H. Up-regulation of HSPA1A and HSPA1B in the blood of tophi patients and its clinical significance. *Acta Biochim. Pol.* **2022**, *69* (4), 781−785.

(23) Gombos, T.; Förhécz, Z.; Pozsonyi, Z.; Jánoskuti, L.; Prohászka, Z. Interaction of serum 70-kDa heat shock protein levels and HspA1B (+1267) gene polymorphism with disease severity in patients with chronic heart failure. *Cell Stress Chaperones* **2008**, *13* (2), 199−206.

(24) Song, Y. J.; Zhong, C. B.; Wang, X. B. Heat shock protein 70: A promising therapeutic target for myocardial ischemia-reperfusion injury. *J. Cell. Physiol.* **2019**, *234* (2), 1190−1207.

(25) Zilaee, M.; Ferns, G. A.; Ghayour-Mobarhan, M. Heat shock proteins and cardiovascular disease. *Adv. Clin. Chem.* **2014**, *64*, 73−115.
(26) Yang, Z.; Zhang, Q.; Yu, H.; Du, H.; Li, L.; He, Y.; Zhu, S.; Li, C.; Zhang, S.; Luo, B.; et al. Genetic association study of a novel indel polymorphism in HSPA1B with the risk of sudden cardiac death in the Chinese populations. *Forensic Sci. Int.* **2021**, *318*, 110637.
(27) Morisson, L.; Duceau, B.; Do Rego, H.; Lancelot, A.; Hariri, G.; Charfeddine, A.; Laferrière-Langlois, P.; Richebé, P.; Lebreton, G.; Provenchère, S.; et al. A new machine learning algorithm to predict veno-arterial ECMO implantation after post-cardiotomy low cardiac output syndrome. *Anaesth. Crit. Care Pain Med.* **2023**, *42* (1), 101172.

https://doi.org/10.1021/acsomega.4c07339
ACS Omega 2025, 10, 637−654